ACS Photonics

pubs.acs.org/journal/apchd5

Article

Optically Pumped Lasing Based on Vibrationally Dressed Exciton Polaritons in a Single-Crystal Molecular Cavity at Room Temperature

Takumi Matsuo,*,¶ Yusuke Ueda, Hitoshi Mizuno, Fumio Sasaki, Kenichi Yamashita, and Hisao Yanagi*,¶

Cite This: https://doi.org/10.1021/acsphotonics.2c00123

Read Online

ACCESS | Metrics & More | Article Recommendations | Supporting Information

ABSTRACT: Polaritonic photonics is one of the key technologies for future quantum-based information and communication. Here, we demonstrate strong evidence of vibrationally dressed exciton polaritons formed in a single-crystal planar cavity of 5,5″-bis(biphenylyl)-2,2′:5′,2″-terthiophene (BP3T) at room temperature. Under optical pumping, the BP3T crystals exhibit longitudinal multimode lasing at the primary and secondary vibronic progression bands based on Fabry–Pérot (F-P) resonation between side facets of the planar cavity. Each gain-narrowed vibronic band extraordinarily split into multiple peaks at excitation fluence around the lasing threshold, accompanied with time delay up to several tens of picoseconds, which is unexplainable for conventional photon lasing. Although those lasing characteristics are primarily interpreted as a regime of exciton-polaritons (EPs), the energy versus wavenumber plots of splitting spectra are well-explained by coupling with cooperative vibrations of the ordered BP3T molecules.

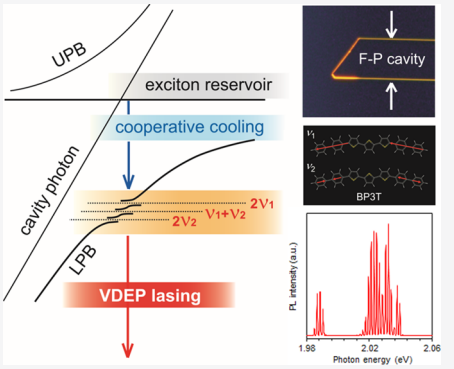

KEYWORDS: *vibrationally dressed exciton polariton, optically pumped laser, thiophene/phenylene co-oligomer, molecular single crystal*

After amplified spontaneous emission (ASE) and lasing have been demonstrated for a variety of organic crystals under optical excitation,[1−10] electrically pumped lasing has been first demonstrated in an organic light-emitting field-effect transistor (OLEFET) with a thiophene/phenylene co-oligomer (TPCO)[11] and subsequently in an organic light-emitting diode (OLED) with distyrylbenzene (DSB) derivatives.[12] In the former OLEFET device, a thin planar single crystal of 5,5″-bis(biphenylyl)-2,2′:5′,2″-terthiophene (BP3T, the molecular structure is shown in Figure 1a) has been used as an active medium, which is capable of transporting both holes and electrons with high mobilities.[13]

Along with superior lasing characteristics owing to thermal stability, high quantum yield, and large refractive index,[14−16] BP3T and other TPCO single crystals have shown unique light amplification behaviors, indicating cooperative processes under optical pumping conditions, as follows: (i) Unusually split lasing spectra with longitudinal multimodes have been observed in Fabry–Pérot (F-P) oscillating conditions.[17] (ii) Pulse-shaped emissions accompanied with time delay from several tens to several hundreds of picoseconds with respect to the excitation pulse origin have been observed at excitation fluence around the lasing threshold.[17,18] This unusually long delay time has been interpreted as build-up time of macroscopically correlated emitters in analogy with superradiance (SR) or superfluorescence (SF).[19−23] (iii) Excitation beam area dependences of gain-narrowing threshold fluence have been observed, which can be related to superfluorescence phenomena.[18,24,25] (iv) Mirrorless lasing based on stimulated resonance Raman scattering (SRRS) has been observed in BP3T and other TPCO single crystals, suggesting a formation of coherent molecular vibrations.[26,27]

Although those unusual light amplification behaviors have been phenomenologically well-investigated for TPCO single crystals, their detailed descriptions have not been well established. Exciton polaritons (EPs) are one of the reliable candidates for those cooperative light emissions as reported for inorganic and organic semiconductor microcavities.[28−31] Polariton lasing, which has been reported also for organic materials,[32] occurs at lower threshold fluence than that of photon lasing based on the stimulated emission (SE) process. Polaritonic behaviors of organic materials have been reported almost for microcavity structures; however, they demand combining fragile organic layers and a pair of distributed Bragg reflectors (DBRs). Recently, it has been reported that EPs can be formed in single-crystal and microstructured organic

Received: January 21, 2022

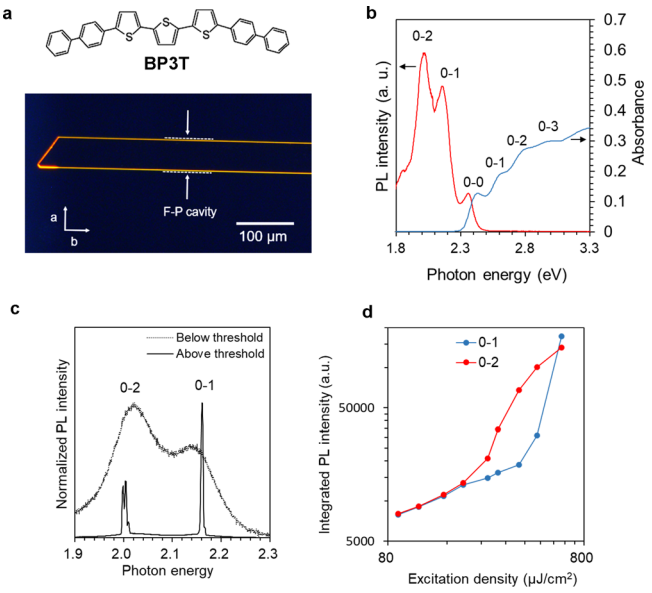

Figure 1. Photoluminescence characteristics of single-crystal BP3T. (a) Molecular structure of BP3T and fluorescence microscopy image of a BP3T single crystal obtained by a modified solution growth process. (b) PL and absorption spectra taken from a BP3T single crystal showing vibronic progressions in 0−0, 0−1, and 0−2 transition bands. (c) PL spectra observed for a BP3T single crystal below and above the light amplification threshold, showing gain-narrowed lasing peaks at the 0−1 and 0−2 bands in the latter condition. (d) Excitation density dependences of integrated PL intensity for the 0−1 and 0−2 bands. Their nonlinear increase onsets indicate lasing threshold fluences of 432 and 240 $\mu J/cm^2$ for the 0−1 and 0−2 bands, respectively.

semiconductors even without external cavities at room temperature, and they are attracting interests as cavity-free polaritonic devices.[33,34] Such cavity-free EPs have been also reported for nano/microstructures with lead halide perovskites, which enable lasing even at CW excitation.[35,36] Besides the formation of EPs, another unique quasi-particle named "vibro-polariton" has been also reported for organic materials, which are formed by strong coupling between molecular vibronic quanta and cavity photons.[37] Moreover, vibrationally dressed exciton polaritons (VDEPs) have been theoretically demonstrated,[38] suggesting that molecular vibronic modes play a key role in the formation of EPs.[39]

Here, we report experimental evidence of cooperative emission attributed to VDEPs in self-organized planar cavities of single-crystal BP3T at room temperature. The obtained F-P mode lasing characteristics under optical pumping are investigated by time-resolved photoluminescence (PL) measurements and discussed in detail using energy versus wavenumber ($E-k$) plots. Extraordinary splitting spectra at vibronic progression bands accompanied with long time delay are attributed to the lower branch of EPs coupled with the intramolecular vibration modes of the BP3T molecule. The observed time delay is interpreted as a build-up duration of VDEPs via cooperative cooling brought by coherent molecular vibrations.

RESULTS

Optically Pumped Lasing in Single-Crystal BP3T. Single-crystal TPCOs have been conventionally grown via physical vapor transport (PVT) based on sublimation under a temperature gradient in inert gas flowing conditions.[6,10,12] However, BP3T single crystals prepared by the PVT method possess curved crystal edges, not ideal to achieving lasing in F-P oscillating modes. Therefore, here we grew BP3T crystals by slight modification of solution growth[40,41] to obtain large and well-shaped single crystals as representatively shown in Figure 1a. According to the X-ray diffraction analysis,[18] the crystal surface is assigned to the (001) plane of the monoclinic form (a = 7.526 Å, b = 5.786 Å, c = 59.997 Å, β = 92.818°, space group: $P2_1/c$)[42] where all the molecular axes of BP3T stand perpendicular to this plane as shown in Figure S1 in the Supporting Information.

The pair of parallel crystal side facets, the length between which is typically on a submillimeter scale, function as F-P mirrors providing a planar single-crystal resonator. As seen in Figure 1a, the emitted light is only observed at the crystal contour edges, indicating that the fluorescence is thoroughly confined in the two-dimensional cavity and no crystal defect is observable. Figure 1b shows absorption and PL spectra observed for a single-crystal BP3T exhibiting several bands corresponding to vibronic progressions of the $\pi-\pi^*$ electronic transition between the highest occupied molecular orbital (HOMO) and lowest unoccupied molecular orbital (LUMO)

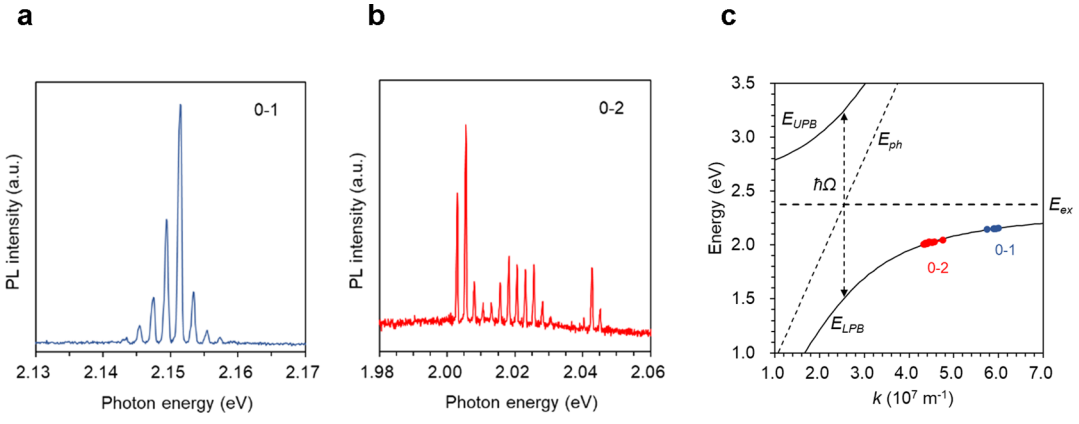

Figure 2. Fabry−Pérot lasing and polariton dispersion. (a,b) High-resolution PL spectra taken above the lasing threshold fluence for the 0−1 and 0−2 bands, respectively. (c) $E-k$ dispersion plots estimated from lasing spectra shown in panels (a) and (b). The plots are fitted with LPB dispersion (E_{LPB}) by coupling between excitons (E_{ex}) and cavity photons (E_{ph}) showing a Rabi splitting energy ($\hbar\Omega$).

https://doi.org/10.1021/acsphotonics.2c00123
ACS Photonics XXXX, XXX, XXX−XXX

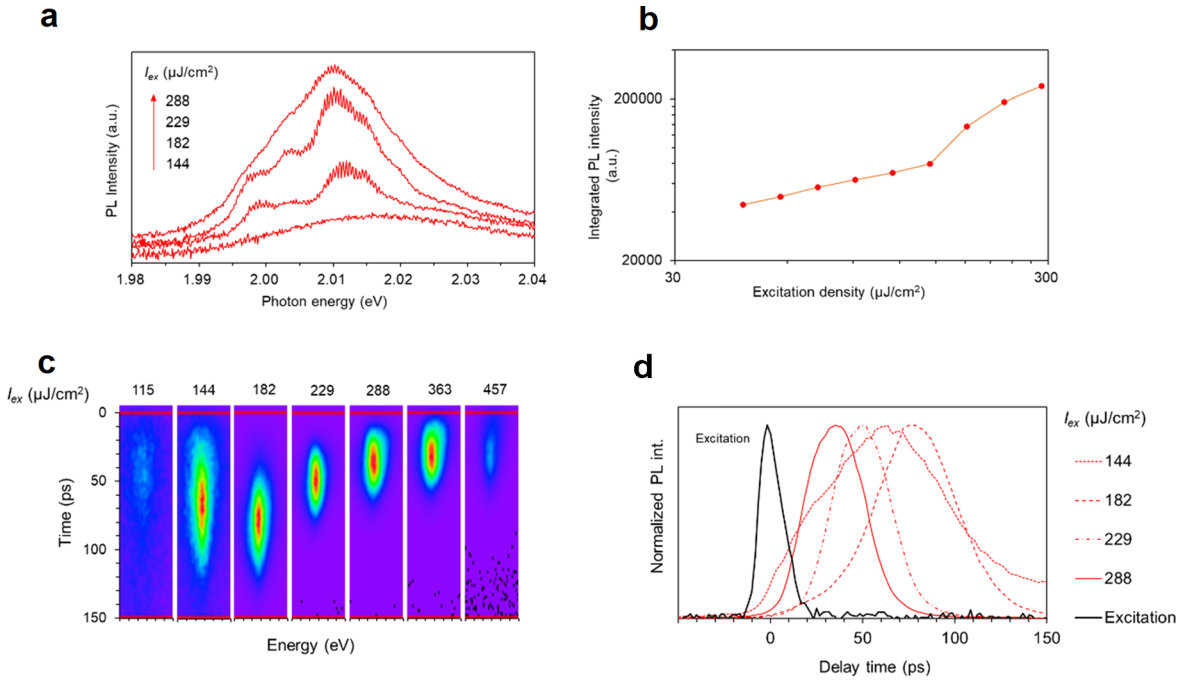

Figure 3. Time-resolved PL spectroscopy in the 0−2 band. Excitation fluence dependence of PL spectra (a) and integrated PL intensities (b). (c) Color maps of time-resolved PL intensities in the 0−2 band at varied excitation fluences. The horizontal axis of each map is graduated in photon energy from 1.98 to 2.04 eV. (d) Time profiles of integrated and normalized PL intensities as a function of excitation fluence.

as shown in Figure S2 in the Supporting Information. Three prominent PL bands at 2.35, 2.15, and 2.02 eV are assigned to the 0−0, 0−1, and 0−2 transitions, respectively. Figure 1c shows PL spectra observed for a BP3T single crystal under optical pumping using a Nd:YAG pulsed laser. The stripe-shaped excitation beam is focused on the crystal surface being perpendicular to the parallel side facets so that only the F-P lasing is detected in this direction. The 0−1 and 0−2 bands are amplified into gain-narrowed peaks at 2.16 and 2.00 eV, respectively, when the excitation fluence is increased beyond a certain threshold. From excitation density dependences of integrated PL intensity shown in Figure 1d, the threshold fluence was determined to be 432 and 240 $\mu J/cm^2$ for the 0−1 and 0−2 peaks, respectively. Note that the gain-narrowing threshold is meaningfully lower for the 0−2 transition, which is related to the contribution of VDEPs in the lasing process as mentioned later.

As respectively shown in Figure 2a,b, high-resolution PL spectra taken above the threshold fluence clearly indicate lasing oscillations for both the 0−1 and 0−2 transitions. From the observed longitudinal multimode intervals (ΔE) and measured cavity length (L), the group refractive index (n_g) values are estimated to be 5.3 and 3.7 for the 0−1 and 0−2 bands, respectively, according to $n_g = hc/(2L\Delta E)$ where h is the Planck constant and c is the speed of light. The obtained n_g values are high enough for efficient light confinement in the planar cavity of BP3T, and the sufficient finesse in the F-P lasing spectra enables us to analyze EP and VDEP characteristics using $E-k$ plots in the subsequent sections.

EP Characterization. Although the F-P lasing spectra in Figure 2a,b are obtained from the same excited position of the measured single crystal, their spectral features are meaningfully different: the mode intensities distribute in a Gaussian envelope in the 0−1 transition band while those in the 0−2 transition show extraordinary splitting into mainly three sub-bands. The former spectral envelope is typical for amplified spontaneous emission (ASE) as well as exciton−polariton emission. On the other hand, the latter splitting with a band width narrower than the thermal broadening at room temperature suggests the existence of resonance other than the F-P oscillation. In order to characterize those spectral origins, $E-k$ plots are derived with $k = 2\pi n_g/\lambda$ where k is the wavenumber in the direction of F-P oscillation, *i.e.*, perpendicular to the side facets of the BP3T single crystal. From the relation between n_g and k, k is expressed as $k = \pi hc/(L\lambda\Delta E)$. Thus, the $E-k$ dispersion is obtained from the ΔE values at each multimode peak wavelength λ for both in the 0−1 and 0−2 lasing bands as shown in Figure 2c. This methodology has been utilized to evaluate EP characteristics for spontaneous emissions from organic single-crystal nanowires.[43]

In order to evaluate EP characteristics, the exciton energy (E_{ex}) is generally determined from the 0−0 absorption peak, which overlaps with the 0−0 PL peak. In the present case of the BP3T single crystal, however, the 0−0 absorption and PL peaks are Stokes-shifted as shown in Figure 1b due to molecular rearrangement in the excited crystal. This Stokes shift energy varies depending on the crystal quality and defects, and the self-absorption effect makes it difficult to precisely determine E_{ex}. Therefore, we adopted the E_{ex} value of 2.376 eV at a mid-position between the absorption and emission peaks as an averaged value. The energy dispersion of cavity photons (E_{ph}) is obtained from $E_{ph} = (\hbar c/n_p)k$ where $\hbar$, c, and n_p are Dirac's constant, speed of light, and phase refractive index of the BP3T single crystal, respectively. Energy dispersions (E_{UPB} and E_{LPB}, respectively) of the upper polariton branch (UPB) and lower polariton branch (LPB) can be derived as a result of strong coupling between the excitons and cavity photons, according to the following equation

https://doi.org/10.1021/acsphotonics.2c00123
ACS Photonics XXXX, XXX, XXX−XXX

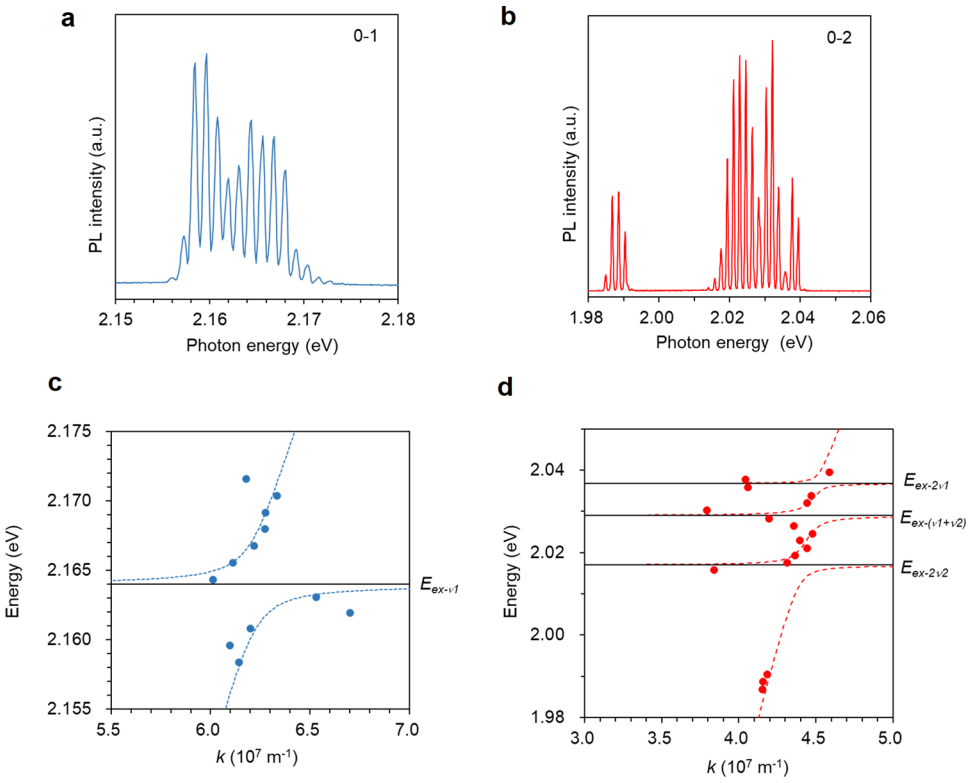

Figure 4. Lasing spectra and VDEP dispersions. (a,b) Lasing spectra showing unusual deformation and splitting in the 0−1 and 0−2 bands, respectively. (c) $E-k$ plots and calculated energy dispersion for the 0−1 band spectrum shown in panel (a). The $E-k$ plots are fitted by coupling of vibrationally dressed exciton with LPB according to eq 2. (d) $E-k$ plots and calculated energy dispersion for the 0−2 band spectrum shown in (b) where vibrationally dressed excitons with secondary vibration modes are included as shown in eq 3.

$$E_{\mathrm{UPB,LPB}} = \frac{1}{2}(E_{\mathrm{ex}} + E_{\mathrm{ph}}) \pm \frac{1}{2}\sqrt{(E_{\mathrm{ex}} - E_{\mathrm{ph}})^2 + (\hbar\Omega)^2} \quad (1)$$

where $\hbar\Omega$ is the Rabi-splitting parameter corresponding to the coupling strength between excitons and cavity photons. Consequently, the $E-k$ dispersion plots are well-fitted as dispersion curves of E_{LPB} as shown in Figure 2c. Light emission from UPB is not observable because the population in UPB is promptly relaxed to the exciton reservoir within sub-picoseconds.[44] The resulting fitting parameters are n_p = 2.11 and $\hbar\Omega$ = 1.74 eV. The obtained n_p is a reasonable value for TPCO crystals,[18] and the $\hbar\Omega$ values estimated for four BP3T single-crystal samples range in 1.54−1.74 eV. Note that the obtained $\hbar\Omega$ is one order of magnitude larger than the exciton energy width, which is roughly ∼100 meV as estimated from Figure 1b, indicating that the excitons are strongly coupled with the cavity photons confined in the single-crystal BP3T. It has been reported that the molecular orientation can strongly enhance the exciton−photon interaction in organic microcavities.[45] The uniaxial alignment of transition dipole moments perpendicular to the cavity plane of the BP3T crystal must be an optimal configuration for the strong coupling with the cavity photons in the transverse magnetic (TM) mode.

Time-Resolved Measurements. For further investigation of lasing characteristics, time-resolved PL measurements were performed under the F-P oscillating condition for the single-crystal BP3T. Figure 3a shows excitation density dependences of PL spectra taken in the 0−2 transition region. Since the spectroscopy resolution is lower and the cavity length (L = 295 μm) of the sample crystal used here is much larger as compared to those in Figure 2, the lasing spectral finesse is worsened by power broadening in particular at higher excitation fluence. However, its band width of ∼20 meV indicates evident gain-narrowing and the fluence dependence of integrated PL intensity clearly demonstrates the lasing threshold as shown in Figure 3b. Figure 3c,d respectively shows the corresponding color maps and time-decay profiles of time-resolved PL intensities integrated and normalized in the measured photon energy range. Around the lasing threshold fluence at 144 μJ/cm^2, the 0−2 PL band starts gain-narrowing and the time profile spreads over 0−150 ps with a maximum intensity around 60 ps with respect to the time origin of the excitation pulse as shown in Figure 3d. When the fluence is increased at 182 μJ/cm^2, the time duration becomes narrow and the maximum intensity appears further delayed at 77 ps. With increasing fluence at 229 and 288 μJ/cm^2, the time profiles become more pulse-shaped while the delay time is getting shorter. Since a typical rising time of optically pumped lasing is a few picoseconds, this delay time is much longer than that expected for photon lasing based on the SE process. Note that the PL spectra in Figure 3a are unusually split into multiple bands at 182 and 229 μJ/cm^2. When the fluence is increased to 288 μJ/cm^2, the splitting spectrum merges to a single band with typical gain spectral width for photon lasing at room temperature while the lasing spectral finesse is worsened by power broadening. Those observed spectral splittings accompanied with time delay suggest a contribution of VDEPs as discussed later.

The fluence-dependent time-resolved lasing features with unusual splitting and time delay are typically observed for the 0−2 band while those of the 0−1 band obtained for most of the single-crystal BP3T samples are different as shown in

https://doi.org/10.1021/acsphotonics.2c00123
ACS Photonics XXXX, XXX, XXX−XXX

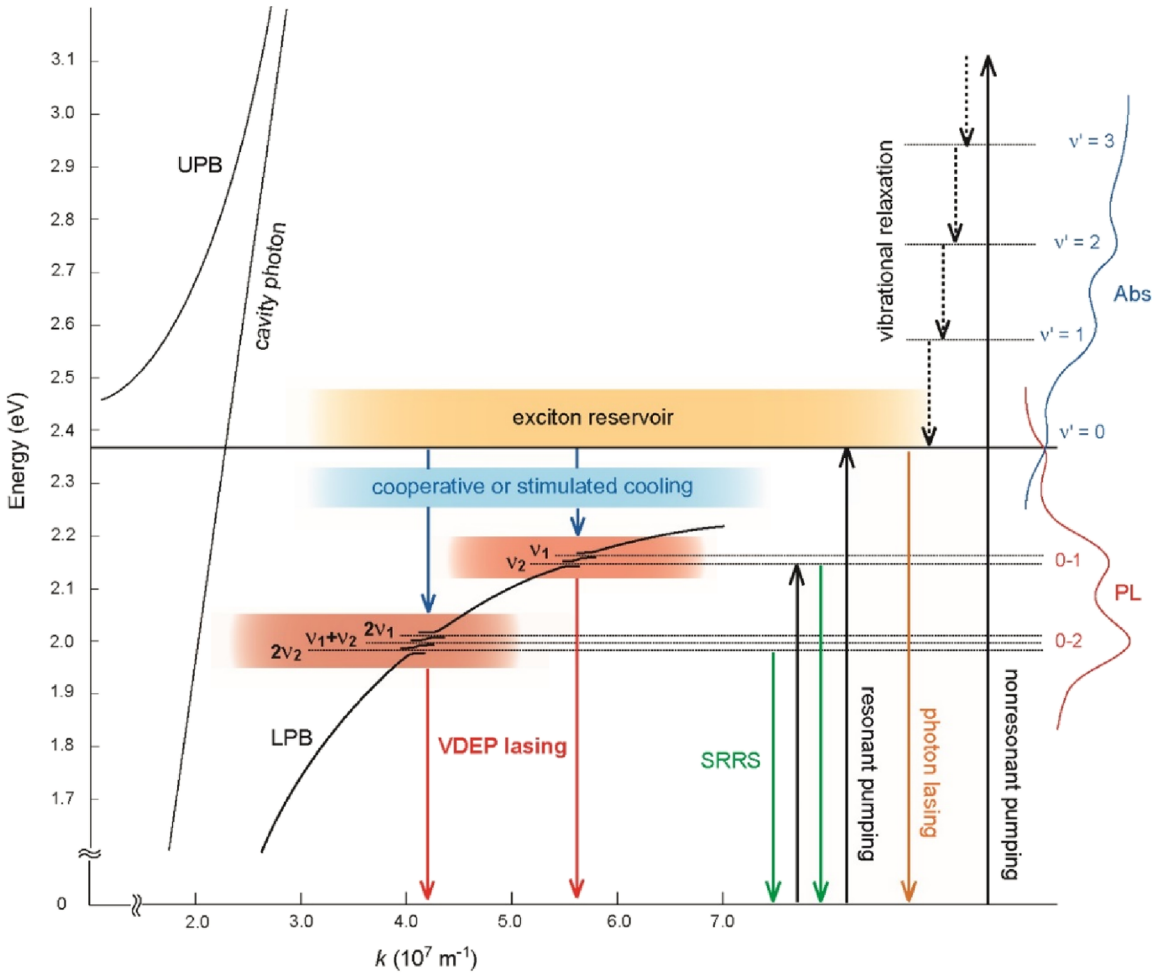

Figure 5. Energy dispersion and formation process of VDEPs. After nonresonant pumping at $\nu' > 3$, excitons are accumulated in the S_1 reservoir via vibrational relaxation. In the formation of EPs by coupling with cavity photons, the excitons are cooled by cooperative or stimulated processes. In the former, the relaxation to LPB occurs via correlated molecular vibrations, resulting in VDEP lasing accompanied with spectral splitting. In the latter, the excitons are relaxed to LPB through stimulated emission of localized intramolecular vibrations without LPB splitting (not shown in the figure). Under resonant pumping, the stimulated vibrational emission gives rise to SRRS.

Figure S3 in the Supporting Information. Independent of excitation fluence around the lasing threshold, the 0−1 spectra appear with a single band at 2.14−2.18 eV and their time-resolved profiles are almost unchanged without long delay time.

VDEP Characterization. Such a difference between the 0−1 and 0−2 bands might be primarily ascribed to a higher Franck−Condon factor for the 0−2 transition (see Figure 1b,c), which gives rise to more effective coupling of the 0−2 excitons with cavity photons. However, the lasing spectra of some samples exhibit unusual deformation or splitting for both the 0−1 and 0−2 bands as shown in Figure 4a,b. The lasing oscillation of the 0−1 band has a wavered intensity envelope while that of the 0−2 band prominently splits into four peaks. Their $E-k$ dispersions calculated for the 0−1 and 0−2 bands are plotted in Figure 4c,d, respectively. Both dispersion plots are not simply fitted by E_{LPB} according to the coupling between excitons and cavity photons. Corresponding to their spectra features, the $E-k$ plots of the 0−1 band exhibit an anti-crossing split and those of the 0−2 band are dispersed into discrete energy levels.

In order to analyze those dispersion data, we have used a coupled oscillator model including vibrationally dressed excitons.[38] In the case of the 0−1 band (Figure 4c), the $E-k$ plots are fitted by coupling among E_{ph}, E_{ex}, and $E_{ex-\nu 1}$, where $E_{ex-\nu 1}$ is the 0−1 emission energy coupled with the primary mode of molecular vibrations. Assuming that one vibrational mode having a frequency ν_1 contributes to the coupling, the corresponding phenomenological Hamiltonian is described as the following 3 × 3 matrix

$$\begin{pmatrix} E_{ph} & \hbar\Omega/2 & \hbar\omega_{\nu 1}/2 \\ \hbar\Omega/2 & E_{ex} & 0 \\ \hbar\omega_{\nu 1}/2 & 0 & E_{ex-\nu 1} \end{pmatrix} \quad (2)$$

where $\hbar\omega_{\nu_1}$ is the coupling parameter of LPB with the vibrationally dressed 0−1 exciton. Using E_{ex} = 2.376 eV, $E_{ex-\nu 1}$ = 2.164, and n_p = 2.11, the anti-crossing dispersion is well-fitted as shown by dotted curves in Figure 4c. The difference between E_{ex} and $E_{ex-\nu 1}$, 0.212 eV, approximately corresponds to the energy of prominent vibration modes of the BP3T molecule shown in Figure S2b in the Supporting Information. As a result, the interaction energies of $\hbar\Omega$ = 1.76 eV and $\hbar\omega_{\nu_1}$ = 7.0 meV are obtained. The $\hbar\Omega$ value is consistent with the Rabi splitting energy obtained for the result shown in Figure 2.

https://doi.org/10.1021/acsphotonics.2c00123
ACS Photonics XXXX, XXX, XXX−XXX

The resultant $\hbar\omega_{\nu_1}$ value is much smaller than the thermal kinetic energy at room temperature (~26 meV). It suggests the existence of additional resonance, which overcomes thermal broadening as we will discuss later.

For fitting the $E-k$ dispersion in the 0−2 emission band shown in Figure 4d, the secondary modes of molecular vibrations are included in the coupled oscillator model as shown in the following phenomenological 5 × 5 Hamiltonian

$$\begin{pmatrix} E_{\mathrm{ph}} & \hbar\Omega/2 & \hbar\omega_{2\nu1}/2 & \hbar\omega_{(\nu1+\nu2)}/2 & \hbar\omega_{2\nu2}/2 \\ \hbar\Omega/2 & E_{\mathrm{ex}} & 0 & 0 & 0 \\ \hbar\omega_{2\nu1}/2 & 0 & E_{\mathrm{ex}-2\nu1} & 0 & 0 \\ \hbar\omega_{(\nu1+\nu2)}/2 & 0 & 0 & E_{\mathrm{ex}-(\nu1+\nu2)} & 0 \\ \hbar\omega_{2\nu2}/2 & 0 & 0 & 0 & E_{\mathrm{ex}-2\nu2} \end{pmatrix} \quad (3)$$

where $E_{\mathrm{ex}-2\nu1}$, $E_{\mathrm{ex}-(\nu1+\nu2)}$, and $E_{\mathrm{ex}-2\nu_2}$ are the energies of vibrationally dressed excitons at the 0−2 emission band. The molecular symmetry of BP3T in the single crystal belongs to the point group of C_{2v},[42] which has two irreducible representations denoted as A_1 and B_1. As shown in Figure S4 in the Supporting Information, the Raman spectrum of a BP3T single crystal taken under off-resonant excitation at room temperature exhibits Raman shifts at ν_1 = 1458 cm^{-1} and ν_2 = 1600 cm^{-1}. These two prominent peaks are both assigned to the B_1 mode with antisymmetric vibrations with respect to the C_2 axis as schematically shown in Figure S2b in the Supporting Information. In the fitting analysis for the 0−2 band dispersion in Figure 4d, the doubled frequency of ν_1 ($E_{\mathrm{ex}-2\nu1}$) and ν_2 ($E_{\mathrm{ex}-2\nu2}$) and the sum-frequency of ν_1 and ν_2 ($E_{\mathrm{ex}-(\nu1+\nu2)}$) are included in the Hamiltonian (3). Accordingly, $\hbar\omega_{2\nu1}$, $\hbar\omega_{2\nu2}$, and $\hbar\omega_{(\nu1+\nu2)}$ are the coupling strengths of LPB with the respective vibrationally dressed excitons. By using the parameters of E_{ex} = 2.351 eV and n_{p} = 2.07, the $E-k$ plots in the 0−2 band are fitted with anti-crossing dispersions as shown with dotted curves in Figure 4d. Note that the resultant E_{ex} value is close to the 0−0 PL peak energy in Figure 1b. It suggests that the E_{ex} value could be more reasonably adopted from the 0−0 PL energy since the cavity photons and vibrational modes are coupled to the excitons relaxed to the S_1 reservoir. The vibrationally dressed exciton energies corresponding to $E_{\mathrm{ex}-2\nu1}$, $E_{\mathrm{ex}-(\nu1+\nu2)}$, and $E_{\mathrm{ex}-2\nu2}$ are estimated to be 2.037, 2.029, and 2.017 eV, respectively. The resulting energy interval between them (8−12 meV) is lower than the energy difference between the ν_1 and ν_2 modes (17.6 meV). This deviation can be mainly attributed to increasing anharmonicity in the secondary vibration mode levels in the 0−2 band. The $\hbar\omega_{2\nu1}$, $\hbar\omega_{2\nu2}$, $\hbar\omega_{(\nu1+\nu2)}$, and $\hbar\Omega$ values are estimated to be 4 meV, 10 meV, 10 meV, and 1.70 eV, respectively. The obtained fitting mostly reproduces the spectral splitting in Figure 4b; however, the experimental plots are somewhat scattered not satisfactorily tracing the anti-crossing dispersion curves. It is probably because the spectral resolution is not enough to accurately determine the E and k values since ΔE between the longitudinal multimodes for the present planar cavity with sub-millimeter L is very small.

DISCUSSION

Based on the experimental results, a plausible scheme for the energy dispersion and formation process of VDEPs in the single-crystal planar cavity of BP3T is summarized in Figure 5. In the present case, the non-resonant optical pumping at λ_{ex} = 355 nm (3.49 eV) or 397 nm (3.12 eV) excites electrons to higher vibrational replicas ($\nu' > 3$) of the singlet Frenkel exciton state (S_1). In a typical organic semiconductor microcavity; thus, generated hot excitons are quickly relaxed to the energy minimum ($\nu' = 0$) of S_1 to form an exciton reservoir, which supplies polariton particles.[46] The excitons in this reservoir can be directly cooled to the polariton state radiatively or via emitting localized molecular vibrations.[38,47] A previous time-resolved and transient spectroscopic study on EPs in vertical microcavities with a single-crystal TPCO derivative has shown two distinguishable polariton renormalization processes, which are attributed to the long-time accumulation in the exciton reservoir (≲100 ps) and ultrafast stimulated polariton cooling (≲1 ps).[48] In the present VDEP process, it is considered that there are additional sub-reservoirs for vibrationally dressed excitons corresponding to each vibronic mode energies in the 0−1 and 0−2 PL bands.

By contrast to the conventional microcavity EPs, we deduce that the excitons accumulated in the main reservoir are cooled via "cooperative" or "stimulated" processes in the single-crystal planar cavity of BP3T. In the cooperative cooling, the renormalization of the LPB states might occur via correlated molecular vibrations, in other words "coherent phonon", among the exciton reservoir molecules. Thus, generated coherent vibrations couple with EPs, which give rise to anti-crossing splits at the respective vibronic states on the LPB dispersion. The observed splitting energies of 7.0 meV for $\hbar\omega_{\nu1}$ in Figure 4c and 4−10 meV for $\hbar\omega_{2\nu1}$, $\hbar\omega_{2\nu2}$, and $\hbar\omega_{(\nu1+\nu2)}$ in Figure 4d evidently prove the existence of additional resonance generated by coherent molecular vibrations, which play a key role in the VDEP formation at room temperature. The measured delay time up to 77 ps can be interpreted as a duration until the hot excitons are populated in the vibrationally dressed exciton states. Such a long rising time is reasonable on the analogy of a cooperative process like superfluorescence where a coherent excited state is built up among excitons, resulting in delayed emission.[20] In the stimulated cooling, on the other hand, the renormalization occurs through stimulated emission of localized intramolecular vibrations, which gives neither spectral splitting nor prominent time delay as the case of LBP in the 0−1 band shown in Figure 2a and Figure S3 in the Supporting Information. In addition, when the system is pumped in resonant at the 0−0 or 0−1 PL band energy, the stimulated vibrational emission results in SRRS, which has been observed for various TPCO single crystals at room temperature and 12 K,[27] as represented in Figure S5 in the Supporting Information.

As seen in the divergence among the spectra presented in Figures 2−4 and Figure S6 in the Supporting Information, the observed VDEP features specially characterized with unusual splitting are varied depending on the morphology and quality of the single-crystal BP3T samples. As representatively shown in Figure S6 in the Supporting Information, the lasing spectra in the 0−1 and 0−2 bands sometimes exhibit more multiply splitting peaks. It suggests that vibration modes other than ν_1 and ν_2 as well as their high-order modes are able to incorporate in the formation of VDEPs since the Raman spectrum taken from the BP3T single crystal (Figure S4 in the Supporting Information) shows many scattering peaks in the frequency range of 700−1400 cm^{-1} under off-resonant excitation. Although the coupling strength of these vibration modes

https://doi.org/10.1021/acsphotonics.2c00123
ACS Photonics XXXX, XXX, XXX−XXX

with excitons might be weaker than those of ν_1 and ν_2, they can also contribute to the formation of VDEPs if the single-crystal cavity quality satisfies the coupling condition.

Another remaining question is whether the F-P feedback resonation in the planar cavity is indispensable for the VDEP formation or not. Figure S7 in the Supporting Information shows an ASE spectrum at room temperature taken from a single-crystal BP3T grown by the PVT method, which has round or curved side edges without parallel mirror facets. Nevertheless, the 0−2 band is split into two peaks, the interval of which is ∼10 meV, approximately corresponding to the energy difference between the ν_1 and ν_2 mode vibrations. It indicates the existence of resonance other than lasing oscillation beyond thermal broadening at room temperature and suggests that the VDEPs may occur in such a planar single-crystal cavity incapable of the F-P lasing.

CONCLUSIONS

The present study has unraveled the clear contribution of VDEPs to cooperatively amplified emissions by using $E-k$ dispersions derived from the multimode F-P lasing in the well-shaped single crystals of BP3T. Such cooperative phenomena based on delocalized excitons over molecules may play a key role in spin-related molecular functions such as thermally assisted delayed fluorescence (TADF)[49] and singlet fission,[50−52] which give advantageous impacts on organic light-emitting and photovoltaic devices. In particular, it is pointed out that the coupling of excitons to molecular vibrations and crystal phonons dominates those physics in molecular semiconductors.[53] In singlet fission, vibrational degrees of freedom coupled to electronic excitation facilitate generation of spin-correlated intermediate pairs of triplet excitons (over-all spin zero) from delocalized multiexcitonic singlets. On the other hand, the delocalization of injected triplet excitons with the aid of vibrational coherence enables the reverse intersystem crossing to over-all singlet excitons in TADF at room temperature. These vibrationally mediated correlations of molecular excitons are evidently demonstrated in the present study through the formation of VDEPs in the single-crystal planar cavity of BP3T. Moreover, the VDEPs could also potentially pave the way for related fields such as molecular-based quantum computing, photochemical reaction control, artificial photosynthesis, and neuroscience of the brain.

METHODS

Sample Preparation. A saturated 1,2,4-trichlorobenzene solution of BP3T was prepared at 190 °C. 10 mL of solution was diluted by adding 2 mL of 1,2,4-trichlorobenzene to remove possibly remaining undissolved BP3T solids. After that, the solution was heated to 190 °C again and successively cooled down to 30−40 °C for 36 h. Afterward, the grown BP3T crystals dispersed in the solution were transferred onto a glass substrate by handling with a metal needle.

Characterization. Absorption spectra were measured using an ultraviolet−visible (UV−vis) spectrometer (JASCO V-530). Fluorescence images as well as PL spectra of single-crystal samples were measured using a fluorescence microscope (Olympus BX-51) equipped with a charge coupled device (CCD) spectrometer (Hamamatsu Photonics PMA-12) through a 10× objective lens. The crystal thickness was confirmed by a surface profiler (Kosaka Laboratory). X-ray diffraction (XRD) measurements were performed by $\theta/2\theta$ scans (Cu Kα, 50 kV, 300 mA). Optically pumped lasing spectra were measured using an excitation source of a Nd:YAG pulsed laser ($\lambda_{3\omega}$ = 355 nm, pulse frequency: 1.2 kHz, pulse duration: 1.1 ns) at room temperature. The excitation beam shaped into a stripe of 0.24 × 0.04 cm^2 through a cylindrical lens was focused on the single crystal surface with an incident angle of ca. 45°. Photoemission radiated from the crystal edge was detected using a CCD spectrometer (Hamamatsu Photonics PMA-50) through an optical fiber. Time-resolved PL spectra were measured using a streak camera (Hamamatsu Photonics C5680) and a Ti:sapphire laser ($\lambda_{2\omega}$ = 397 nm, 150 fs pulse duration, 1 kHz repetition) as an optical excitation source. Off-resonant Raman spectroscopy was carried out using a laser Raman spectrometer (JASCO NRS4100) at an excitation wavelength of 785 nm.

ASSOCIATED CONTENT

Supporting Information

The Supporting Information is available free of charge at https://pubs.acs.org/doi/10.1021/acsphotonics.2c00123.

Crystal structure of BP3T, molecular orbital calculation, and additional spectral data (PDF)

AUTHOR INFORMATION

Corresponding Authors

Takumi Matsuo − *School of Environmental Science and Engineering, Kochi University of Technology, Kami, Kochi 782-8502, Japan*; Email: matsuo.takumi@kochi-tech.ac.jp

Hisao Yanagi − *Graduate School of Science and Technology, Nara Institute of Science and Technology (NAIST), Nara 630-0192, Japan*; orcid.org/0000-0001-8193-0768; Email: yanagi@ms.naist.jp

Authors

Yusuke Ueda − *Faculty of Electrical Engineering and Electronics, Kyoto Institute of Technology, Kyoto 606-8585, Japan*

Hitoshi Mizuno − *Graduate School of Science and Technology, Nara Institute of Science and Technology (NAIST), Nara 630-0192, Japan*

Fumio Sasaki − *Research Institute for Advanced Electronics and Photonics, National Institute of Advanced Industrial Science and Technology, Tsukuba, Ibaraki 305-8568, Japan*

Kenichi Yamashita − *Faculty of Electrical Engineering and Electronics, Kyoto Institute of Technology, Kyoto 606-8585, Japan*; orcid.org/0000-0002-2471-3916

Complete contact information is available at: https://pubs.acs.org/10.1021/acsphotonics.2c00123

Author Contributions

¶T. M. and H. Y. contributed equally to this work.

Funding

F. S., K. Y., and H. Y. received funding from the Japanese Society for the Promotion of Science (JSPS) KAKENHI No. 19H02172. H. M., K. Y., and H. Y. received funding from the Japanese Society for the Promotion of Science (JSPS) KAKENHI No. 20KK0088. T. M. received a grant-in-aid from the Graduate School of Science and Technology, Nara Institute of Science and Technology. T. M. was also supported by the Innovation School from the National Institute of Advanced Industrial Science and Technology.

Notes

The authors declare no competing financial interest.

■ ACKNOWLEDGMENTS

The authors thank Mr. S. Katao, Nara Institute of Science and Technology for XRD measurements. Thanks are also due to Mr. Y. Mekata, Nara Institute of Science and Technology for Raman spectroscopy measurements.

■ REFERENCES

(1) Fichou, D.; Delysse, S.; Nunzi, J.-M. First evidence of stimulated emission from a monolithic organic single crystal: α-Octithiophene. *Adv. Mater.* **1997**, *9*, 1178−1181.
(2) Horowitz, G.; Valat, P.; Garnier, F.; Kouki, F.; Wintgens, V. Photoinduced spontaneous and stimulated emission in sexithiophene single crystals. *Opt. Mater.* **1998**, *9*, 46−52.
(3) Ichikawa, M.; Hibino, R.; Inoue, M.; Haritani, T.; Hotta, S.; Araki, K.; Koyama, T.; Taniguchi, Y. Laser oscillation in monolithic molecular single crystals. *Adv. Mater.* **2005**, *17*, 2073−2077.
(4) Ichikawa, M.; Nakamura, K.; Inoue, M.; Mishima, H.; Haritani, T.; Hibino, R.; Koyama, T.; Taniguchi, Y. Photopumped laser oscillation and charge-injected luminescence from organic semiconductor single crystals of a thiophene/phenylene co-oligomer. *Appl. Phys. Lett.* **2005**, *87*, 221113.
(5) Yamao, T.; Yamamoto, K.; Taniguchi, Y.; Miki, T.; Hotta, S. Laser oscillation in a highly anisotropic organic crystal with a refractive index of 4.0. *J. Appl. Phys.* **2008**, *103*, No. 093115.
(6) Kanazawa, S.; Ichikawa, M.; Koyama, T.; Taniguchi, Y. Self-waveguided photoemission and lasing of organic crystalline wires obtained by an improved expitaxial growth method. *Chem. Phys. Chem.* **2006**, *7*, 1881−1884.
(7) Mizuno, H.; Haku, U.; Marutani, Y.; Ishizumi, A.; Yanagi, H.; Sasaki, F.; Hotta, S. Single crystals of 5,5′-Bis(4′-methoxybiphenyl-4-yl)-2,2′-bithiophene for organic laser media. *Adv. Mater.* **2012**, *24*, 5744−5749.
(8) Varghese, S.; Yoon, S.-J.; Casado, S.; Fischer, R. C.; Wannemacher, R.; Park, S.-Y.; Gierschner, J. Orthogonal resonator modes and low lasing threshold in highly emissive distyrylbenzene-based molecular crystals. *Adv. Opt. Mater.* **2014**, *2*, 542−548.
(9) Mizuno, H.; Maeda, T.; Yanagi, H.; Katsuki, H.; Aresti, M.; Quochi, F.; Saba, M.; Mura, A.; Bongiovanni, G.; Sasaki, F.; Hotta, S. Optically pumped lasing from single crystals of a cyano-substituted thiophene/phenylene co-oligomer. *Adv. Opt. Mater.* **2014**, *2*, 529−534.
(10) Gierschner, J.; Varghese, S.; Park, S.-Y. Organic single crystal lasers: A materials view. *Adv. Opt. Mater.* **2016**, *4*, 348−364.
(11) Kanagasekaran, T.; Shimotani, H.; Kasai, K.; Onuki, S.; Kavthe, R. D.; Kumashiro, R.; Hiroshiba, N.; Jin, T.; Asao, N.; Tanigaki, K. Towards electrically driven organic semiconductor laser with field-effective transistor structure. *arXiv*:1903.08869.
(12) Sandanayaka, A. S. D.; Matsushima, T.; Bencheikh, F.; Terakawa, S.; Potscavage, W. J., Jr.; Qin, C.; Fujihara, T.; Goushi, K.; Ribierre, J.-C.; Adachi, C. Indication of current-injection lasing from an organic semiconductor. *Appl. Phys. Express* **2019**, *12*, No. 061010.
(13) Bisri, S. Z.; Takenobu, T.; Yomogida, Y.; Shimotani, H.; Yamao, T.; Hotta, S.; Iwasa, Y. High mobility and luminescent efficiency in organic single-crystal light-emitting transistors. *Adv. Funct. Mater.* **2009**, *19*, 1728−1735.
(14) Yamao, T.; Okuda, Y.; Makino, Y.; Hotta, S. Dispersion of the refractive indices of thiophene/phenylene co-oligomer single crystals. *J. Appl. Phys.* **2011**, *110*, No. 053113.
(15) Yamao, T.; Sakamoto, N.; Hotta, S.; Mizuno, H.; Yanagi, H. Refractive index measurements of well-defined polygon crystals of thiophene/phenylene co-oligomers. *Jpn. J. Appl. Phys.* **2012**, *51*, No. 11PD03.
(16) Takahashi, W.; Maruyama, K.; Li, J.; Imakawa, M.; Takenobu, T. Optical characteristic of 5,5″-bis(4-biphenylyl)-2,2′:5′,2″-terthiophene single-crystal thin-film resonator. *Jpn. J. Appl. Phys.* **2014**, *53*, No. 02BB02.
(17) Yanagi, H.; Marutani, Y.; Sasaki, F.; Makino, Y.; Yamao, T.; Hotta, S. Prethreshold lasing with time-delayed pulse emission from a single crystal of thiophene/phenylene co-oligomer. *Appl. Phys. Express* **2011**, *4*, No. 062601.
(18) Matsuo, T.; Mizuno, H.; Sasaki, F.; Yanagi, H. Indication of cooperative light amplification in 5,5″-bis(4-biphenylyl)−2,2′:5,2″-terthiophene single crystals at room temperature. *Jpn. J. Appl. Phys.* **2020**, *59*, SDDB02.
(19) Dicke, R. H. Coherence in spontaneous radiation processes. *Phys. Rev.* **1954**, *93*, 99−110.
(20) Florian, R.; Schwan, L. O.; Schmid, D. Time-resolving experiments on Dicke superfluorescence of O2- centers in KCl. Two-color super fluorescence. *Phys. Rev. A* **1984**, *29*, 2709−2715.
(21) Rainò, G.; Becker, M. A.; Bodnarchuk, M. I.; Mahrt, R. F.; Kovalenko, M. V.; Stöferle, T. Superfluorescence from lead halide perovskite quantum dot superlattices. *Nature* **2018**, *563*, 671−675.
(22) Meinardi, F.; Cerminara, M.; Sassella, A.; Bonifacio, R.; Tubino, R. Superradiance in molecular H aggregates. *Phys. Rev. Lett.* **2003**, *91*, No. 247401.
(23) Frolov, S. V.; Vardeny, Z. V.; Yoshino, K. Cooperative and stimulated emission in poly(p-phenylene-vinylene) thin films and solutions. *Phys. Rev. B* **1998**, *57*, 9141−9147.
(24) Hiramatsu, T.; Matsuoka, N.; Yanagi, H.; Sasaki, F.; Hotta, S. Gain-narrowed emissions of thiophene/phenylene co-oligomer single crystals. *Phys. Status Solidi C* **2009**, *6*, 338−341.
(25) Shang, H.; Shimotani, H.; Ikeda, S.; Kanagasekaran, T.; Oniwa, K.; Jin, T.; Asao, N.; Yamamoto, Y.; Tamura, H.; Abe, K.; Kanno, M.; Yoshizawa, M.; Tanigaki, K. Comparative study of single and dual gain-narrowed emission in thiophene/furan/phenylene co-oligomer single crystals. *J. Phys. Chem. C* **2017**, *121*, 2364−2368.
(26) Yanagi, H.; Yoshiki, A.; Hotta, S.; Kobayashi, S. Stimulated resonance Raman scattering from single crystals of a thiophene/phenylene co-oligomer. *Appl. Phys. Lett.* **2003**, *83*, 1941−1943.
(27) Yanagi, H.; Marutani, Y.; Matsuoka, N.; Hiramatsu, T.; Ishizumi, A.; Sasaki, F.; Hotta, S. Resonant stimulation of Raman scattering from single-crystal thiophene/phenylene co-oligomers. *Appl. Phys. Lett.* **2013**, *103*, 243301.
(28) Deng, H.; Weihs, G.; Santori, C.; Bloch, J.; Yamamoto, Y. Condensation of semiconductor microcavity exciton polaritons. *Science* **2002**, *298*, 199−202.
(29) Kasprzak, J.; Richard, M.; Kundermann, S.; Baas, A.; Jeambrun, P.; Keeling, J. M. J.; Marchetti, F. M.; Szymańska, M. H.; André, R.; Staehli, J. L.; Savona, V.; Littlewood, P. B.; Deveaud, B.; Dang, L. S. Bose−Einstein condensation of exciton polaritons. *Nature* **2006**, *443*, 409−414.
(30) Weisbuch, C.; Nishioka, M.; Ishikawa, A.; Arakawa, Y. Observation of the coupled exciton-photon mode splitting in a semiconductor quantum microcavity. *Phys. Rev. Lett.* **1992**, *69*, 3314−3317.
(31) Lidzey, D. G.; Bradley, D. D. C.; Skolnick, M. S.; Virgili, T.; Walker, S.; Whittaker, D. M. Strong exciton-photon coupling in an organic semiconductor microcavity. *Nature* **1998**, *395*, 53−55.
(32) Kéna-Cohen, S.; Forrest, S. R. Room-temperature polariton lasing in an organic single-crystal microcavity. *Nat. Photonics* **2010**, *4*, 371−375.
(33) Tang, J.; Zhang, J.; Lv, Y.; Wang, H.; Xu, F. F.; Zhang, C.; Sun, L.; Yao, J.; Zhao, Y. S. Room temperature exciton−polariton Bose−Einstein condensation in organic single-crystal microribbon cavities. *Nat. Commun.* **2021**, *12*, 3265.
(34) Pandya, R.; Chen, R. Y. S.; Gu, Q.; Sung, J.; Schnedermann, C.; Ojambati, O. S.; Chikkaraddy, R.; Gorman, J.; Jacucci, G.; Onelli, O. D.; Willhammar, T.; Johnstone, D. N.; Collins, S. M.; Midgley, P. A.; Auras, F.; Baikie, T.; Jayaprakash, R.; Mathevet, F.; Soucek, R.; Du, M.; Alvertis, A. M.; Ashoka, A.; Vignolini, S.; Lidzey, D. G.; Baumberg, J. J.; Friend, R. H.; Barisien, T.; Legrand, L.; Chin, A. W.; Yuen-Zhou, J.; Saikin, S. K.; Kukura, P.; Musser, A. J.; Rao, A. Microcavity-like exciton-polaritons can be the primary photo-

https://doi.org/10.1021/acsphotonics.2c00123
ACS Photonics XXXX, XXX, XXX−XXX

excitation in bare organic semiconductors. *Nat. Commun.* **2021**, *12*, 6519.
(35) Shang, Q.; Li, M.; Zhao, L.; Chen, D.; Zhang, S.; Chen, S.; Gao, P.; Shen, C.; Xing, J.; Xing, G.; Shen, B.; Liu, X.; Zhang, Q. Role of the exciton-polariton in a continuous-wave optically pumped $CsPbBr_3$ perovskite laser. *Nano Lett.* **2020**, *20*, 6636−6643.
(36) Zhang, Q.; Shang, Q.; Su, R.; Do, T. T. H.; Xiong, Q. Halide perovskite semiconductor lasers: Materials, cavity design, and low threshold. *Nano Lett.* **2021**, *21*, 1903−1914.
(37) Long, J. P.; Simpkins, B. S. Coherent coupling between a molecular vibration and Fabry-Pérot optical cavity to give hybridized states in the strong coupling limit. *ACS Photonics* **2015**, *2*, 130−136.
(38) Spano, F. C. Exciton−phonon polaritons in organic microcavities: Testing a simple ansatz for treating a large number of chromophores. *J. Chem. Phys.* **2020**, *152*, 204113.
(39) Coles, D. M.; Michetti, P.; Clark, C.; Tsoi, W. C.; Adawi, A. M.; Kim, J. S.; Lidzey, D. G. Vibrationally assisted polariton-relaxation processes in strongly coupled organic-semiconductor microcavities. *Adv. Funct. Mater.* **2011**, *21*, 3691−3696.
(40) Yamao, T.; Miki, T.; Akagami, H.; Nishimoto, Y.; Ota, S.; Hotta, S. Direct formation of thin single crystals of organic semiconductors onto a substrate. *Chem. Mater.* **2007**, *19*, 3748−3753.
(41) Inada, Y.; Yamao, T.; Inada, M.; Itami, T.; Hotta, S. Giant organic single-crystals of a thiophene/phenylene co-oligomer toward device applications. *Synth. Met.* **2011**, *161*, 1869−1877.
(42) Hotta, S.; Goto, M.; Azumi, R.; Inoue, M.; Ichikawa, M.; Taniguchi, Y. Crystal structures of thiophene/phenylene co-oligomers with different molecular shapes. *Chem. Mater.* **2004**, *16*, 237−241.
(43) Liao, Q.; Xu, Z.; Zhong, X.; Dang, W.; Shi, Q.; Zhang, C.; Weng, Y.; Li, Z.; Fu, H. An organic nanowire waveguide exciton−polariton sub-microlaser and its photonic application. *J. Mater. Chem. C* **2014**, *2*, 2773−2778.
(44) Virgili, T.; Coles, D.; Adawi, A. M.; Clark, C.; Michetti, P.; Rajendran, S. K.; Brida, D.; Polli, D.; Cerullo, G.; Lidzey, D. G. Ultrafast polariton relaxation dynamics in an organic semiconductor microcavity. *Phys. Rev. B* **2011**, *83*, No. 245309.
(45) Ishii, T.; Bencheikh, F.; Forget, S.; Chénais, S.; Heinrich, B.; Kreher, D.; Sosa Vargas, L.; Miyata, K.; Onda, K.; Fujihara, T.; Kéna-Cohen, S.; Mathevet, F.; Adachi, C. Enhanced light-matter interaction and polariton relaxation by the control of molecular orientation. *Adv. Opt. Mater.* **2021**, *9*, 2101048.
(46) Michetti, P.; La Rocca, G. C. Exciton-phonon scattering and photoexcitation dynamics in J-aggregate microcavities. *Phys. Rev. B: Condens. Matter Mater. Phys.* **2009**, *79*, No. 035325.
(47) Litinskaya, M.; Reineker, P.; Agranovich, V. M. Fast polariton relaxation in strongly coupled organic microcavities. *J. Lumin.* **2004**, *110*, 364−372.
(48) Yamashita, K.; Huynh, U.; Richter, J.; Eyre, L.; Deschler, F.; Rao, A.; Goto, K.; Nishimura, T.; Yamao, T.; Hotta, S.; Yanagi, H.; Nakayama, M.; Friend, R. H. Ultrafast dynamics of polariton cooling and renormalization in an organic single-crystal microcavity under nonresonant pumping. *ACS Photonics* **2018**, *5*, 2182−2188.
(49) Uoyama, H.; Goushi, K.; Shizu, K.; Nomura, H.; Adachi, C. Highly efficient organic light-emitting diodes from delayed fluorescence. *Nature* **2012**, *492*, 234−238.
(50) Smith, M. B.; Michl, J. Singlet fission. *Chem. Rev.* **2010**, *110*, 6891−6936.
(51) Musser, A. J.; Liebel, M.; Schnedermann, C.; Wende, T.; Kehoe, T. B.; Rao, A.; Kukura, P. Evidence for conical intersection dynamics mediating ultrafast singlet exciton fission. *Nat. Phys.* **2015**, *11*, 352−357.
(52) Bakulin, A. A.; Morgan, S. E.; Kehoe, T. B.; Wilson, M. W. B.; Chin, A. W.; Zigmantas, D.; Egorova, D.; Rao, A. Real-time observation of multiexcitonic states in ultrafast singlet fission using coherent 2D electronic spectroscopy. *Nat. Chem.* **2016**, *8*, 16−23.
(53) Alvertis, A. M.; Pandya, R.; Muscarella, L. A.; Sawhney, N.; Nguyen, M.; Ehrler, B.; Rao, A.; Friend, R. H.; Chin, A. W.; Monserrat, B. Impact of exciton delocalization on exciton-vibration interactions in organic semiconductors. *Phys. Rev. B* **2020**, *102*, No. 081122(R).

https://doi.org/10.1021/acsphotonics.2c00123
ACS Photonics XXXX, XXX, XXX−XXX